A Comparison of Two Types of Macro Basis Functions Defined on LEGO Electromagnetic Bricks

A Comparison of Two Types of Macro Basis Functions Defined on LEGO Electromagnetic Bricks

V. Lancellotti[1], R. Maaskant[2],
[1]Eindhoven University of Technology, Eindhoven, The Netherlands, v.lancellotti@tue.nl
[2]Chalmers University of Technology, Gothenburg, Sweden, rob.maaskant@chalmers.se

***Abstract*—Linear embedding via Green's operators (LEGO) is a domain decomposition method that uses electromagnetic "bricks" to solve wave scattering problems. The algebraic form of the relevant functional equations (which are derived by invoking the surface equivalence principle) is a linear system characterized by a full and possibly large matrix. The size of the system can be effectively reduced by adopting macro basis functions defined on the surface of a brick through 1) the eigencurrents expansion method (EEM) and 2) the Adaptive Cross Approximation (ACA). The two methods lead to the same results, though the ACA macro basis functions are faster to compute.**

I. Introduction

Linear embedding via Green's operators (LEGO) is a domain decomposition method particularly well-suited for the solution of electromagnetic (EM) scattering problems comprised of many objects immersed in a background medium [1] and a host medium [2]. The formulation is based on the introduction of simple-shaped EM bricks $\mathcal{D}_k$, $k = 1, \ldots, N_D$, each one enclosing an object, as illustrated in Fig. 1. The EM behaviour of a brick is accounted for through its scattering operator S_{kk}, viz.,

$$q_k^{\mathrm{s}} = \mathsf{S}_{kk}\, q_k^{\mathrm{i}}, \tag{1}$$

where q_k^{i} and q_k^{s} are abstract column vectors of equivalent incident and scattered surface currents on $\partial\mathcal{D}_k$, namely,

$$q_k^{\mathrm{i}} = \begin{bmatrix} \mathbf{J}_k^{\mathrm{i}}\sqrt{\eta_1} \\ -\mathbf{M}_k^{\mathrm{i}}/\sqrt{\eta_1} \end{bmatrix}, \quad q_k^{\mathrm{s}} = \begin{bmatrix} \mathbf{J}_k^{\mathrm{s}}\sqrt{\eta_1} \\ -\mathbf{M}_k^{\mathrm{s}}/\sqrt{\eta_1} \end{bmatrix}, \tag{2}$$

with η_1 the intrinsic impedance of the background medium (①). The multiple scattering phenomenon that occurs between any two bricks is described by means of transfer operators T_{kn}, T_{nk}, $n \neq k$. The functional equation governing the EM problem can be shown to be [1]

$$(\mathsf{I} - \mathrm{diag}\,\{\mathsf{S}_{kk}\}\,\mathsf{T})\, q^{\mathrm{s}} = \mathrm{diag}\,\{\mathsf{S}_{kk}\}\, q^{\mathrm{i}}, \tag{3}$$

where I is a suitable identity operator, and T is the total transfer operator given explicitly, e.g., in [3, Eq. (12)].

The numerical inversion of (3) relies on the Method of Moments (MoM) in Galerkin's form. The procedure starts with the definition of sets of Rao-Wilton-Glisson (RWG) functions on $\partial\mathcal{D}_k$ to represent $q_k^{\mathrm{s,i}}$ and on the surface of the object inside $\mathcal{D}_k$ to expand the surface currents thereon [1]. Next, the scattering and transfer operators are turned into their algebraic counterparts, i.e., $[S_{kk}]$ and $[T_{kn}]$. With these two ingredients, the weak form of (3), namely,

$$([I] - \mathrm{blkdiag}\,\{[S_{kk}]\}\,[T])\,[q^{\mathrm{s}}] = \mathrm{blkdiag}\,\{[S_{kk}]\}\,\left[q^{\mathrm{i}}\right], \tag{4}$$

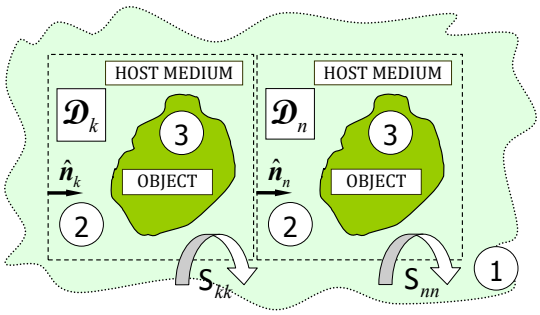

Fig. 1: LEGO method applied to a set of objects: each object (medium ①) is enclosed inside an EM brick $\mathcal{D}_k$, $k = 1, \ldots, N_D$, in turn described by means of a scattering operator S_{kk}. In this paper, the host medium (②) and background material (①) are assumed to have the same EM parameters.

can be assembled in a straightforward manner. If the total number of basis functions on $\partial\mathcal{D}_k$ is $2N_F$, the size of the system matrix in (4) is $2N_F N_D$.

In this paper, we describe and compare two sets of macro basis functions, namely, the eigencurrents [1, 3] and functions obtained by applying the adaptive cross approximation (ACA) [4, 5] algorithm to $[S_{kk}]$. Both approaches are viable and effective when $[S_{kk}]$ is rank deficient. This usually happens when the background medium (①) and the host medium (②) have the same EM properties (see Fig. 1).

II. Derivation of the macro basis functions

In this section we outline the compression of (4) by means of two reduced vector bases for representing the unknown expansion coefficients $[q^{\mathrm{s}}]$.

A. Order reduction with ACA of $[S_{kk}]$

The discrete version of the ACA algorithm [5] allows us to factorize the algebraic scattering operators as

$$[S_{kk}] = [U_{kk}]\,[V_{kk}]\,, \tag{5}$$

where the matrices $[U_{kk}]$ and $[V_{kk}]$ have size $2N_F \times r_k$ and $r_k \times 2N_F$, respectively. From (1) and (5) we derive that

$$[q_k^{\mathrm{s}}] = [U_{kk}]\,[V_{kk}]\,\left[q_k^{\mathrm{i}}\right] = [U_{kk}]\,[c_k]\,, \tag{6}$$

which suggests the columns of $[U_{kk}]$ can be adopted as a vector basis to represent the scattered current coefficients $[q_k^{\mathrm{s}}]$, because $r_k \ll 2N_F$. Besides, in the light of (6) the columns of $[U_{kk}]$ define entire-domain macro basis functions over the surface of $\partial\mathcal{D}_k$.

It is convenient to define the block-diagonal matrices

$$[U] = \text{blkdiag}\left\{[U_{kk}]\right\}, \quad [V] = \text{blkdiag}\left\{[V_{kk}]\right\} \tag{7}$$

to lighten the notation. Upon inserting (5) into (4) and letting

$$[q^{\text{s}}] = [U]\,[\tilde{q}^{\text{s}}], \qquad [\tilde{q}^{\text{i}}] = [V]\,[q^{\text{i}}], \tag{8}$$

after a little algebra we obtain the compressed linear system

$$([I] - [V]\,[T]\,[U])\,[\tilde{q}^{\text{s}}] = [\tilde{q}^{\text{i}}], \tag{9}$$

whose rank is $\sum_k r_k$ in general or $N_D r_1$ in the case where all the bricks are identical.

B. Order reduction with eigencurrents of $[S_{kk}]$ revisited

The spectral decomposition of the algebraic scattering operators reads [1]

$$[S_{kk}] = [E_{kk}]\,\text{diag}\left\{\lambda_p^{(k)}\right\}[E_{kk}]^{-1}, \tag{10}$$

where we have adopted the non-standard notation $[E_{kk}]$ to avoid confusion with $[V_{kk}]$ in (5). The definition (1) in tandem with (10) suggests that a basis for $[q_k^{\text{s}}]$ can be formed by using the first N_C columns of $[E_{kk}]$, i.e., the eigenvectors associated with the largest eigenvalues[1]. The eigenvectors in turn define entire-domain macro basis functions (dubbed eigencurrents) over the surface of $\partial\mathcal{D}_k$ [1].

To proceed, we introduce the block-diagonal matrices

$$[U_C] = \text{blkdiag}\left\{[U_C^{(k)}]\right\}, [V_C] = \text{blkdiag}\left\{[V_C^{(k)}]\right\}, \tag{11}$$

where $[U_C^{(k)}]$ ($[V_C^{(k)}]$) is a matrix formed with the first N_C columns (rows) of $[E_{kk}]$, ($[E_{kk}]^{-1}$). Thanks to these definitions and by further letting

$$[q^{\text{s}}] = [U_C]\,[\tilde{q}^{\text{s}}], \qquad [\tilde{q}^{\text{i}}] = [V_C]\,[q^{\text{i}}], \tag{12}$$

with a few manipulations the compressed form of (4) becomes

$$([I_C] - [\Lambda_C]\,[V_C]\,[T]\,[U_C])\,[\tilde{q}^{\text{s}}] = [\Lambda_C]\,[\tilde{q}^{\text{i}}], \tag{13}$$

where

$$[\Lambda_C] = \text{blkdiag}\left\{\text{diag}\left\{\lambda_p^{(k)}\right\}\right\}, \quad p = 1, \ldots, N_C, \tag{14}$$

is a diagonal matrix formed with the first N_C eigenvalues of each scattering operator $[S_{kk}]$. The rank of (13) is $N_D N_C$ under the assumption that all the bricks are identical.

III. Results and Discussion

We have investigated the properties of the eigencurrents and the ACA macro basis functions by solving a few plane-wave scattering problems. The background (①) and the host medium (②) are free space in all the tests considered.

The first configuration consists of a cluster of four spheres arranged in a square lattice, and the spheres (medium ③) are assumed to be either PEC or dielectric. The LEGO model is comprised of $N_D = 4$ cubic bricks, and the number of RWG functions over $\partial\mathcal{D}_k$ is $2N_F = 648$. The RWG functions over the surface of a sphere are $N_O = 294$ for the PEC case and twice as many for the dielectric case. (Additional data are given in Fig. 2.) The Radar Cross Sections (RCS) obtained by solving (9) and (13) are compared in Fig. 2. We have set the number of eigencurrents to $N_C = 50$. From Fig. 2 it is seen that, for the case of PEC spheres, $r_1 = N_A = 63$ ACA macro basis functions are necessary to attain the same level of accuracy; this corresponds to a threshold $t = 10^{-3}$ for stopping the ACA of $[S_{11}]$. The dielectric case is expected to be less demanding, and indeed $r_1 = N_A = 25$ ($t = 10^{-2}$) ACA macro basis functions are sufficient to attain the same accuracy afforded by $N_C = 50$ eigencurrents. For the sake of completeness, the scattered currents q_k^{s} over the surface of the bricks are compared in Figs. 3 and 4. As can be seen the results yielded by the EEM and the ACA functions are in excellent agreement. Finally, plotted in Figs. 5a and 5b are the spectrum of eigenvalues of $[S_{11}]$ and the relative error of the ACA of $[S_{11}]$ [5]. The exponential decay of $|\lambda_p^{(1)}|$ and that of the error are remarkably similar, and this provides a solid argument for the adoption of either the eigencurrents or the ACA macro basis functions for expanding q_k^{s}.

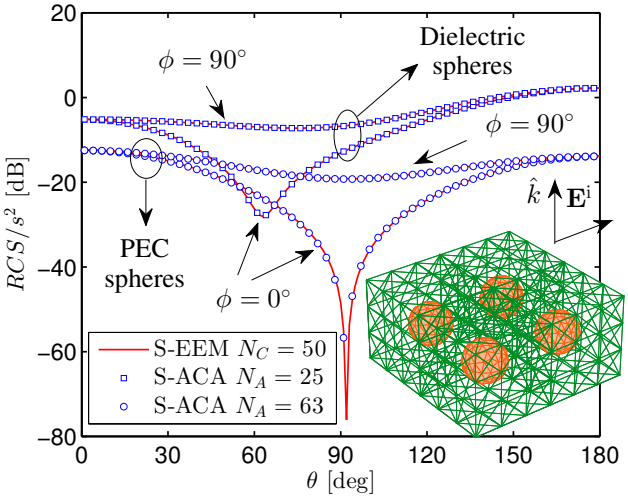

Fig. 2: RCS of four spheres computed with LEGO by using (—) eigencurrents of $[S_{11}]$ and (□, ○) ACA basis of $[S_{11}]$, $t \in \{10^{-3}, 10^{-2}\}$. Inset: LEGO model showing the mesh of the bricks and the spheres, and the incident plane wave. *Data*: radius of the spheres $a = 0.25$ m, edge of the cubic EM bricks $s = 1$ m, incident plane wave $\mathbf{E}^{\text{i}} = \hat{\mathbf{x}}\exp(-\text{j}k_1 z)$, $k_1 = 2\pi f/c_0$, $f = 0.1$ GHz, $\varepsilon_1 = \varepsilon_2 = \varepsilon_0$, $\varepsilon_3 \in \{2\varepsilon_0, \infty\}$.

In the second test case, we have considered four dielectric cylinders embedded in as many cubic bricks arranged in a square lattice. The size of the cylinders is kept fixed whereas the permittivity is varied. The RWG functions over $\partial\mathcal{D}_k$ are $2N_F = 1152$ and the RWG functions over the cylinders are $N_O = 702$. (Additional data are given in Fig. 6.) The RCSs obtained with the two reduction methods are compared in Fig. 6. Since the cylinders are relatively large as compared to the size of the embedding bricks, both the number of coupled eigencurrents and the number of ACA functions are substantial, but the strategy based on the ACA of $[S_{11}]$ is still competitive. The spectrum of $[S_{11}]$ and the relative error of the

[1]This viewpoint is different than the one hinged on the notion of coupled/uncoupled eigencurrents [1], though more in line with Section II-A.

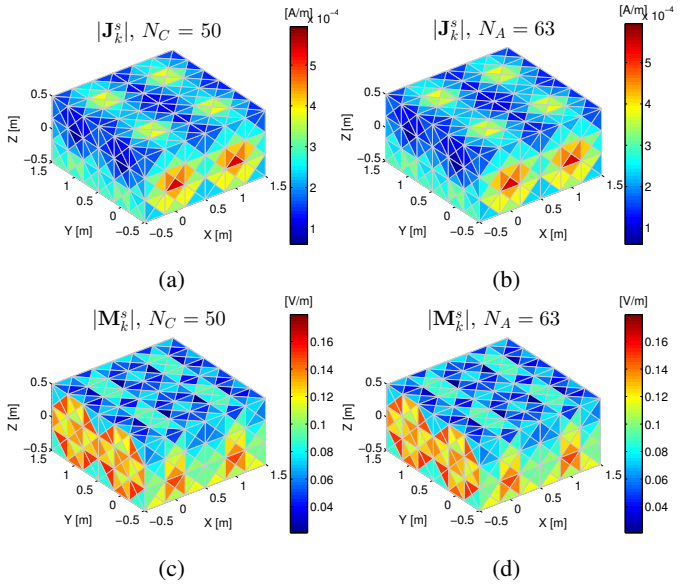

Fig. 3: Scattering from four PEC spheres with LEGO (see inset of Fig. 2): (a), (c) $|\mathbf{J}_k^s|$ and $|\mathbf{M}_k^s|$ computed with eigencurrents of $[S_{11}]$; (b), (d) $|\mathbf{J}_k^s|$ and $|\mathbf{M}_k^s|$ computed with ACA of $[S_{11}]$. *Data*: see Fig. 2.

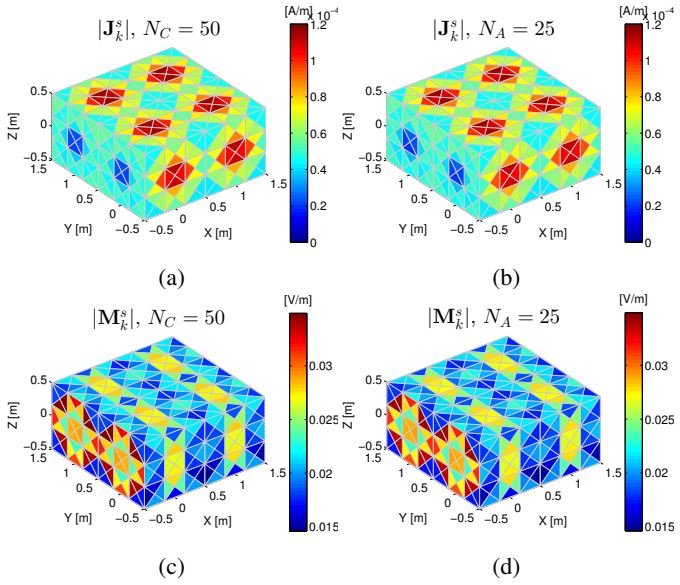

Fig. 4: Scattering from four dielectric spheres with LEGO (see inset of Fig. 2): (a), (c) $|\mathbf{J}_k^s|$ and $|\mathbf{M}_k^s|$ computed with eigencurrents of $[S_{11}]$; (b), (d) $|\mathbf{J}_k^s|$ and $|\mathbf{M}_k^s|$ computed with ACA of $[S_{11}]$. *Data*: see Fig. 2.

ACA of $[S_{11}]$ are compared in Fig. 7. The decay of the ACA error is not monotonic, and this explains why, for a given threshold $t = 10^{-3}$ the number of ACA functions required for the high contrast case ($\varepsilon_3 = 11\varepsilon_0$) is slightly smaller than that for the low contrast case ($\varepsilon_3 = 2\varepsilon_0$). Interestingly, both the spectrum and the error exhibit an abrupt change for $p = r = 576 = N_F$, which is half the number of RWG functions on $\partial\mathcal{D}_k$. This behaviour suggests that, regardless of the reduction strategy adopted, N_F is the maximum number of (any) macro basis functions on the boundary, although this may not always be evident (e.g., [6]). From a physical

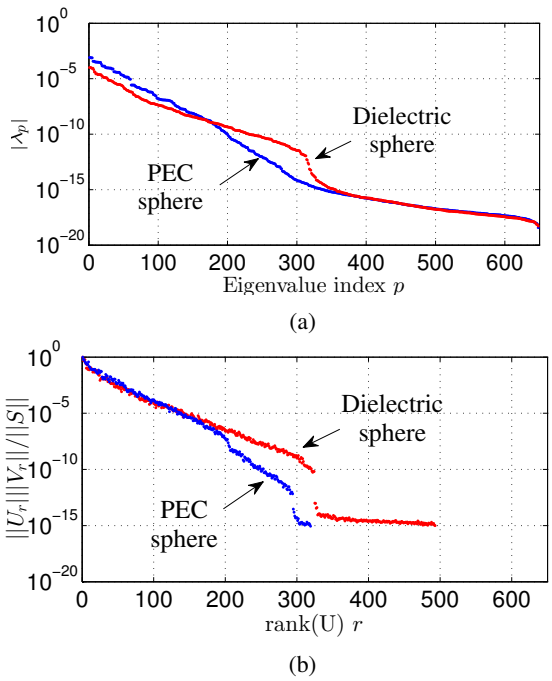

Fig. 5: Comparison of spectrum and ACA of $[S_{11}]$: (a) eigenvalues versus their index; (b) relative error of the ACA decomposition versus $\mathrm{rank}([U_{11}])$.

standpoint, this may be a consequence of the surface equivalent currents $\mathbf{J}_k^s$ and $\mathbf{M}_k^s$ being dependent on each other.

Next, we have examined the scattering from four dielectric cylinders with fixed permittivity but varying sizes. The cylinders are embedded in four cubic bricks arranged in a square lattice. The larger cylinders are the same as those shown in the inset of Fig. 6, while the smaller ones are shown in the inset of Fig. 8. The number of RWG functions over $\partial\mathcal{D}_k$ is again $2N_F = 1152$, but the number of RWG functions over the cylinders has been adjusted according to the size, namely, $N_O \in \{702, 558\}$. The RCSs obtained with the two reduction methods are compared in Fig. 8. As expected, the solution of the case of smaller cylinders requires fewer eigencurrents and ACA functions. As a matter of fact, it can be seen from Fig. 9 the both the eigenvalues of $[S_{11}]$ and the ACA error decay faster for the configuration of smaller cylinders. Besides, the ACA approach is invariably competitive over the EEM strategy.

TABLE I: COMPARISON OF CPU TIMES

Content of LEGO bricks	$2N_F$	T_{ACA} [s]	T_{EEM} [s]
Sphere† $\varepsilon_3 = \infty$ (Fig. 2)	648	0.078	27
Sphere* $\varepsilon_3 = 2\varepsilon_0$ (Fig. 2)	648	0.015	28
Cylinder† $\varepsilon_3 = 2\varepsilon_0$ (Fig. 6)	1152	2.9	20
Cylinder† $\varepsilon_3 = 11\varepsilon_0$ (Fig. 6)	1152	2.4	20
Cylinder† $h = 8$ mm (Fig. 8)	1152	2.5	20
Cylinder† $h = 4$ mm (Fig. 8)	1152	0.43	26

†Threshold for stopping the ACA of $[S_{11}]$ $t = 10^{-3}$

*Threshold for stopping the ACA of $[S_{11}]$ $t = 10^{-1}$

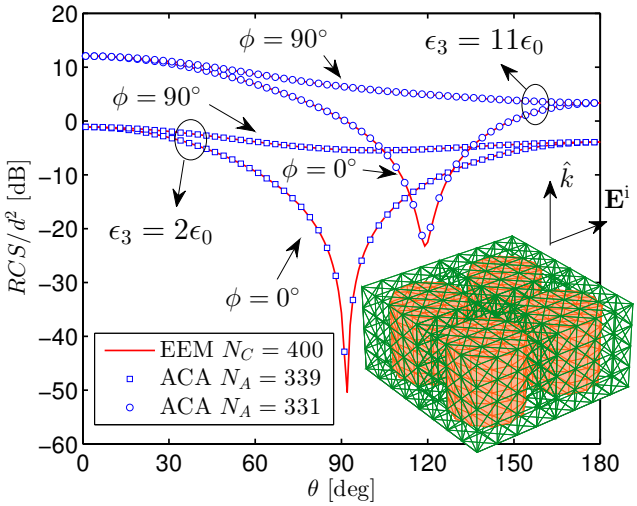

Fig. 6: RCS of four cylinders computed with LEGO by using (—) eigencurrents of $[S_{11}]$ and (□, ○) ACA basis of $[S_{11}]$, $t = 10^{-3}$. Inset: LEGO model showing the mesh of the bricks and the cylinders, and the incident plane wave. *Data*: radius of the cylinder $a = 4$ mm, height of the cylinder 8 mm, edge of the cubic EM bricks $d = 10$ mm, incident plane wave $\mathbf{E}^{\mathrm{i}} = \hat{\mathbf{x}}\exp(-\mathrm{j}k_1 z)$, $k_1 = 2\pi f/c_0$, $f = 7.5$ GHz, $\varepsilon_1 = \varepsilon_2 = \varepsilon_0$, $\varepsilon_3 \in \{2\varepsilon_0, 11\varepsilon_0\}$.

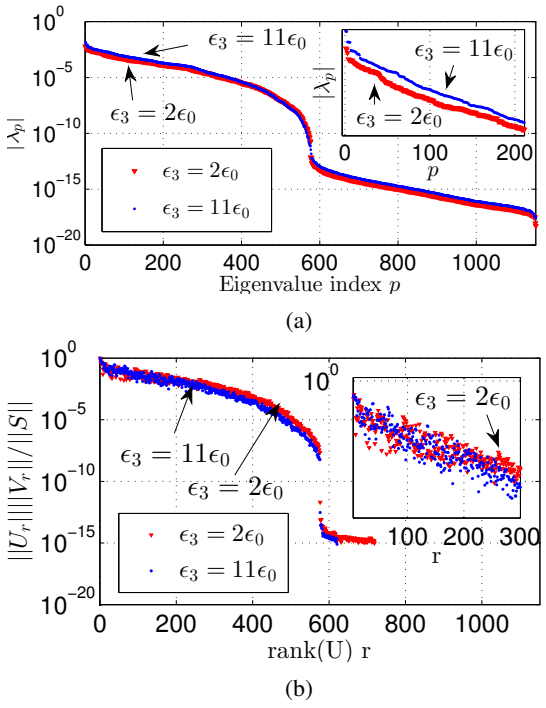

Fig. 7: Comparison of spectrum and ACA of $[S_{11}]$: (a) eigenvalues versus their index; (b) relative error of the ACA decomposition versus $\mathrm{rank}([U_{11}])$.

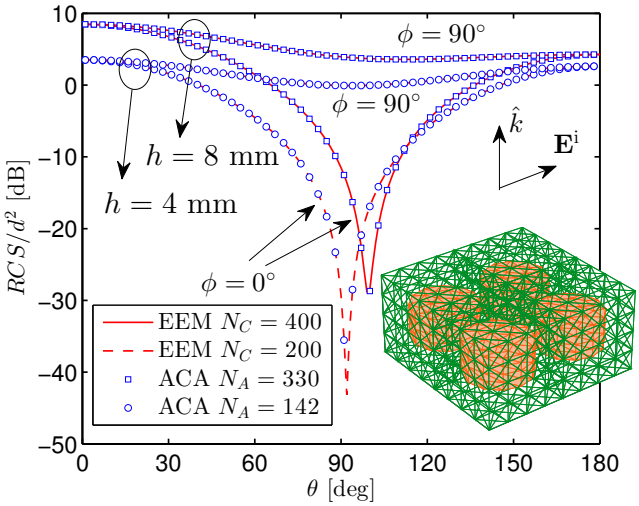

Fig. 8: RCS of four cylinders computed with LEGO by using (—, −−) eigencurrents of $[S_{11}]$ and (□, ○) ACA basis of $[S_{11}]$, $t = 10^{-3}$. Inset: LEGO model showing the mesh of the bricks and the shorter cylinders, and the incident plane wave. *Data*: radius of the cylinder $a = 4$ mm, height of the cylinder $h \in \{4, 8\}$ mm, edge of the cubic EM bricks $d = 10$ mm, incident plane wave $\mathbf{E}^{\mathrm{i}} = \hat{\mathbf{x}}\exp(-\mathrm{j}k_1 z)$, $k_1 = 2\pi f/c_0$, $f = 7.5$ GHz, $\varepsilon_1 = \varepsilon_2 = \varepsilon_0$, $\varepsilon_3 = 6\varepsilon_0$.

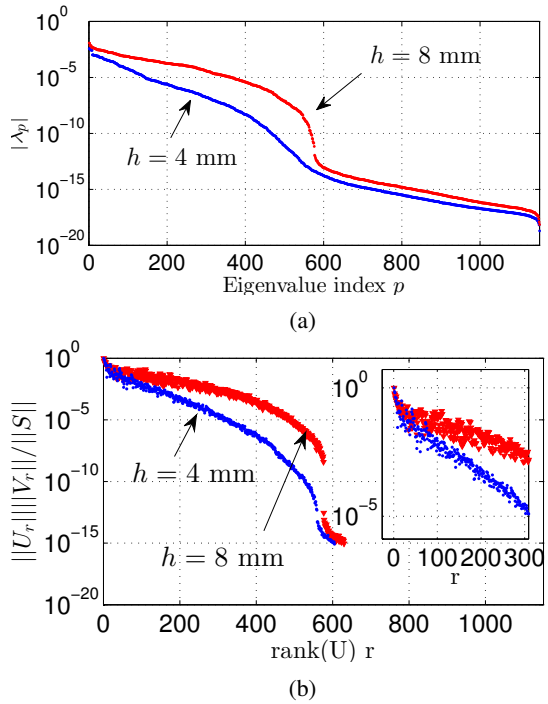

Fig. 9: Comparison of spectrum and ACA of $[S_{11}]$: (a) eigenvalues versus their index; (b) relative error of the ACA decomposition versus $\mathrm{rank}([U_{11}])$.

Compared in Table I are the times taken to perform the spectral decomposition (T_{EEM}) and the ACA (T_{ACA}) of $[S_{11}]$ for the problems of Figs. 2, 6 and 8. As long as all the eigenvectors of $[S_{11}]$ are computed, T_{EEM} is expected to be constant for a given brick type. On the other hand, T_{ACA} varies depending on the effective rank of $[S_{11}]$.

In the last example, we have computed the scattering from a 5×5 array of PEC double cross dipoles arranged in a planar square lattice, as is suggested by the inset of Fig. 10. The dipoles are embedded in $N_D = 25$ cuboidal bricks (see Fig. 11) on which $2N_F = 1080$ RWG functions are introduced, so the size of the uncompressed algebraic system (4) is $2N_F N_D = 27000$. The number of RWG functions over the two dipoles in a brick is $N_O = 554$. (Additional data are given in Fig. 10.) The bistatic RCS obtained with the two

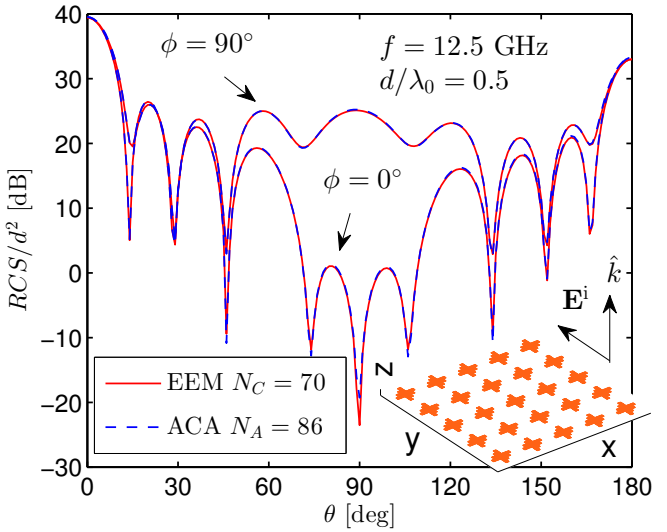

Fig. 10: RCS of an array of double cross dipoles computed with LEGO by using (—) eigencurrents of $[S_{11}]$ and (−−) ACA basis of $[S_{11}]$, $t = 10^{-3}$. Inset: LEGO model showing the double cross dipoles and the incident plane wave. *Data*: length of the dipoles $d = 12$ mm, width of the dipoles 2 mm, horizontal separation and edge of the cubic EM bricks $s = 20$ mm, vertical separation 2 mm, incident plane wave $\mathbf{E}^{\mathrm{i}} = \hat{\mathbf{y}} \exp(-\mathrm{j}k_1 z)$, $k_1 = 2\pi f/c_0$, $f = 12.5$ GHz, $\varepsilon_1 = \varepsilon_2 = \varepsilon_0$, $\varepsilon_3 = \infty$.

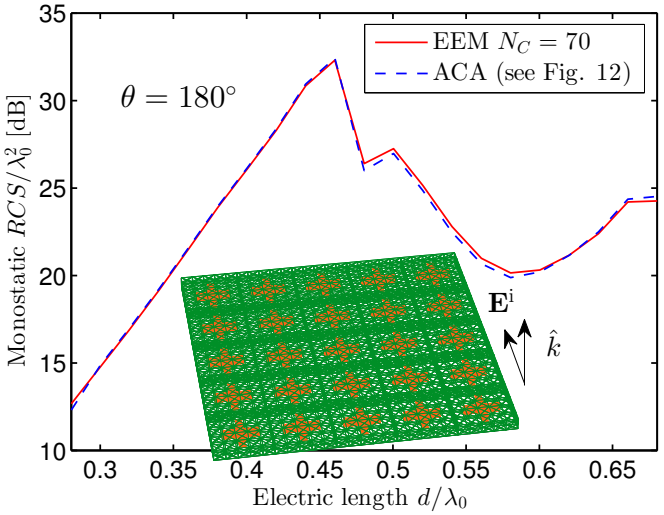

Fig. 11: Monostatic RCS of an array of double cross dipoles computed with LEGO by using (—) eigencurrents of $[S_{11}]$ and (−−) ACA basis of $[S_{11}]$, $t = 10^{-3}$. Inset: LEGO model showing the mesh of the bricks and the dipoles, and the incident plane wave. *Data*: see Fig. 10.

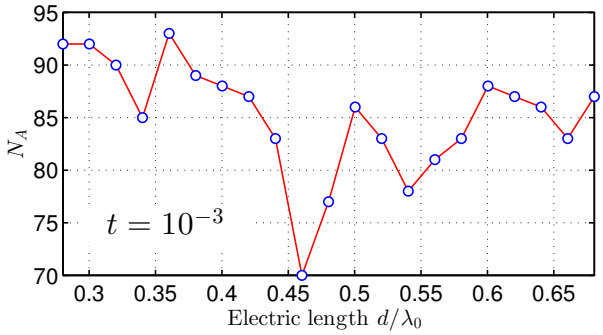

Fig. 12: Number of macro basis functions $N_A = \mathrm{rank}([U_{11}])$ versus electric length for the array of cross dipoles of Figs. 10 and 11.

reduction methods is plotted in Fig. 10 for $f = 12.5$ GHz. At this specific frequency, it appears that fewer eigencurrents are required than ACA functions for the two methods to yield same results. However, $N_C = 70$ eigencurrents may not be sufficient as the frequency of the incident plane wave is increased. This is apparent from Fig. 11 in which the monostatic RCS of the array for $\theta = 180°$ is plotted versus the electric length of the dipoles: for frequencies beyond the resonance ($d/\lambda_0 \approx 0.5$) the RCS predicted by the two methods is not in perfect agreement, although the comparison is still very good. The number of ACA functions for a given threshold $t = 10^{-3}$ is not constant with the frequency, as can be seen in Fig. 12, and this may due to the oscillatory nature of the ACA error. Even though the number of ACA functions in this example is larger than the number of eigencurrents employed, still even in the worst case ($f = 9$ GHz, $N_A = 96$ in Fig. 12) the time taken to carry out the ACA of $[S_{11}]$ is just 0.17 s versus the 20 s spent to determine the spectral decomposition of $[S_{11}]$.

IV. Conclusion

The results point to the ACA macro basis functions as a fast alternative to the EEM, when both strategies are applicable, because carrying out the ACA of $[S_{kk}]$ is indisputably faster than computing the eigenvectors thereof. The numerical experiments considered indicate that the number of ACA functions required for a given level of accuracy increases with the size and the permittivity of the object embedded in a LEGO brick, while there seems to be no clear trend as the frequency is varied. Further investigation is needed to find a link — if any exists — between the threshold t for stopping the ACA of $[S_{kk}]$ and the accuracy of the computed currents q_k^s. A similar study was conducted for the EEM in [6].

References

[1] V. Lancellotti, B. P. de Hon, and A. G. Tijhuis, "An eigencurrent approach to the analysis of electrically large 3-D structures using linear embedding via Green's operators," *IEEE Trans. Antennas Propag.*, vol. 57, no. 11, pp. 3575–3585, Nov. 2009.

[2] ——, "Scattering from large 3-D piecewise homogeneous bodies through linear embedding via Green's operators and Arnoldi basis functions," *Progress In Electromagnetics Research*, vol. 103, pp. 305–322, April 2010.

[3] V. Lancellotti and D. Melazzi, "Hybrid LEGO-EFIE method applied to antenna problems comprised of anisotropic media," *Forum in Electromagnetic Research Methods and Application Technologies (FERMAT)*, vol. 6, 2014, www.e-fermat.org.

[4] M. Bebendorf, "Approximation of boundary element matrices," *Numer. Matematik*, vol. 86, no. 4, pp. 565-589, 2000.

[5] K. Zhao, M. Vouvakis, and J.-F. Lee, "The adaptive cross approximation algorithm for accelerated method of moments computations of EMC problems," *IEEE Trans. Electromag. Compat.*, vol. 47, no. 4, pp. 763–773, Nov. 2005.

[6] V. Lancellotti, B. P. de Hon, and A. G. Tijhuis, "On the convergence of the eigencurrent expansion method applied to linear embedding via Green's operators (LEGO)," *IEEE Trans. Antennas Propag.*, vol. 58, no. 10, pp. 3231–3238, Oct. 2010.